Available online at www.sciencedirect.com
ScienceDirect
Remote Sensing of Environment 112 (2008) 482–495
Remote Sensing of Environment
www.elsevier.com/locate/rse

Assessment of an Urban Sensor View Model for thermal anisotropy

J.A. Voogt

Department of Geography, University of Western Ontario, London ON, Canada N6A 5C2

Received 8 September 2006; received in revised form 8 May 2007; accepted 10 May 2007

Abstract

The surface-sensor-sun relations model (SUM) of Soux et al. [Soux, C.A., Voogt, J.A., & Oke, T.R. (2004). A model to calculate what a remote sensor 'sees' of an urban surface. *Boundary-Layer Meteorology, 111*, 109–132.] is modified to include a coupling of SUM with the actual building structure of a study area, thereby allowing variable building heights and shapes to be represented within SUM as well as the provision for an inter-building spacing that provides a more realistic urban block structure in the internal SUM urban surface representation. Model simulations using both modifications are performed and compared with airborne observations of surface temperature made over a Light Industrial area and a downtown area of Vancouver, BC. The results are generally good, although there is a general tendency to underestimate the overall thermal anisotropy. Use of mean facet temperatures in the validation limits validation statistics for one study area; improvements are made when facet temperatures are updated from individual flight lines. Performing a sensitivity analyses on the contributions to the thermal anisotropy suggests that surface structure and microscale temperature variability both make substantial contributions to the total anisotropy. This finding underscores the importance of including microscale temperature variability in assessments of urban thermal anisotropy. Full hemispheric plots of directional temperature and statistics for each study area are presented as an application of the model and show smooth variations in directional temperature when averaged over the study area.

Keywords: Urban surface temperature; Thermal anisotropy; Sensor view model

1. Introduction

Thermal remote sensors viewing urban areas must consider directional variations of upwelling thermal radiation. These variations are the result of microscale temperature patterns created by the three-dimensional urban surface structure. This directional variation is termed the effective thermal anisotropy of the surface. Effective thermal anisotropy arises because of macroscale surface structure and temperature patterns, rather than the non-lambertian behaviour of individual surface components. The effective thermal anisotropy is an impediment to the application of thermal remote sensors over urban areas because it implies the measurements are biased by view direction and time, and therefore not fully representative of the thermal state of the surface. In recognition of this problem, it has been common practice to limit the viewing angle of remote thermal observations over urban areas to nadir or near-nadir angles, thereby providing measurements restricted primarily to the horizontal surface components of the urban area. This may be termed a "birds-eye" or plan-view of the urban surface (Voogt & Oke, 1997). While this perspective provides a first-order approach to normalizing thermal remote measurements over urban areas, it remains a biased measurement that does not fully account for the three-dimensional structure of the surface. Further, it limits the utility of some remote sensors with significant off-nadir scanning capabilities.

In order to better understand urban thermal anisotropy, observational or modeling approaches may be used. Direct observations of urban thermal anisotropy are difficult to acquire relative to those over other microscale surface covers such as crops, where low towers and standard infrared thermometers may be used to sample representative areas of the surface type of interest (e.g. see the review by Paw U, 1992). Observations of urban anisotropy typically require aircraft based sensors to provide suitable spatial resolution and control over viewing direction, although towers have been used in some select cases (Soux et al., 2004). Examples of direct observation of urban thermal anisotropy include those of Iino and Hoyano (1996), Nichol (1998), Voogt and Oke (1998a) and Lagouarde et al. (2004). These studies have demonstrated the

E-mail address: javoogt@uwo.ca.

0034-4257/$ - see front matter © 2007 Elsevier Inc. All rights reserved.
doi:10.1016/j.rse.2007.05.013

large absolute magnitude – up to 10 °C in highly urbanized districts – of urban thermal anisotropy, where anisotropy is taken to represent the maximum difference in sensor observed temperature from any two view directions.

The high costs associated with direct observations of urban thermal anisotropy generally preclude assessments of multiple land uses, different cities, detailed temporal variations, especially of night-time versus daytime effects, or seasonal variations. To expand our knowledge, the construction of numerical models that can represent the urban thermal anisotropy is needed. One model explicitly developed to assess urban thermal anisotropy is the SUM surface-sensor-sun relations model Soux et al. (2004). This model calculates how a remote sensor views a simple urban surface by calculating the radiative source area or view factors of the urban surface components for a given remote sensor position. The model design is sufficiently flexible to be used for a range of scales. At the microscale, the model can provide radiative source area assessment (Oke, 2004; Schmid, 1997) for tower mounted hemispherical radiometers common to surface micrometeorological measurements. Radiative source area analysis can be used to assess the impact of the surface structure on, for example, net radiation (Offerle et al., 2003) or the matching between radiative and turbulent flux source areas (Schmid, 1997, Voogt & Oke, 2003). At larger scales, when combined with surface temperature information, the model is able to estimate the anisotropy of radiative temperature as seen by a given sensor-sun-surface configuration.

The objectives of this paper are to:

- evaluate the performance of the SUM 3-D directional sensor view model for two urban land use areas;
- investigate the sensitivity of the model results to the representation of the urban surface structure and microscale temperature variability;
- use the model to investigate the full anisotropic distribution of upwelling thermal radiation over the two land use areas.

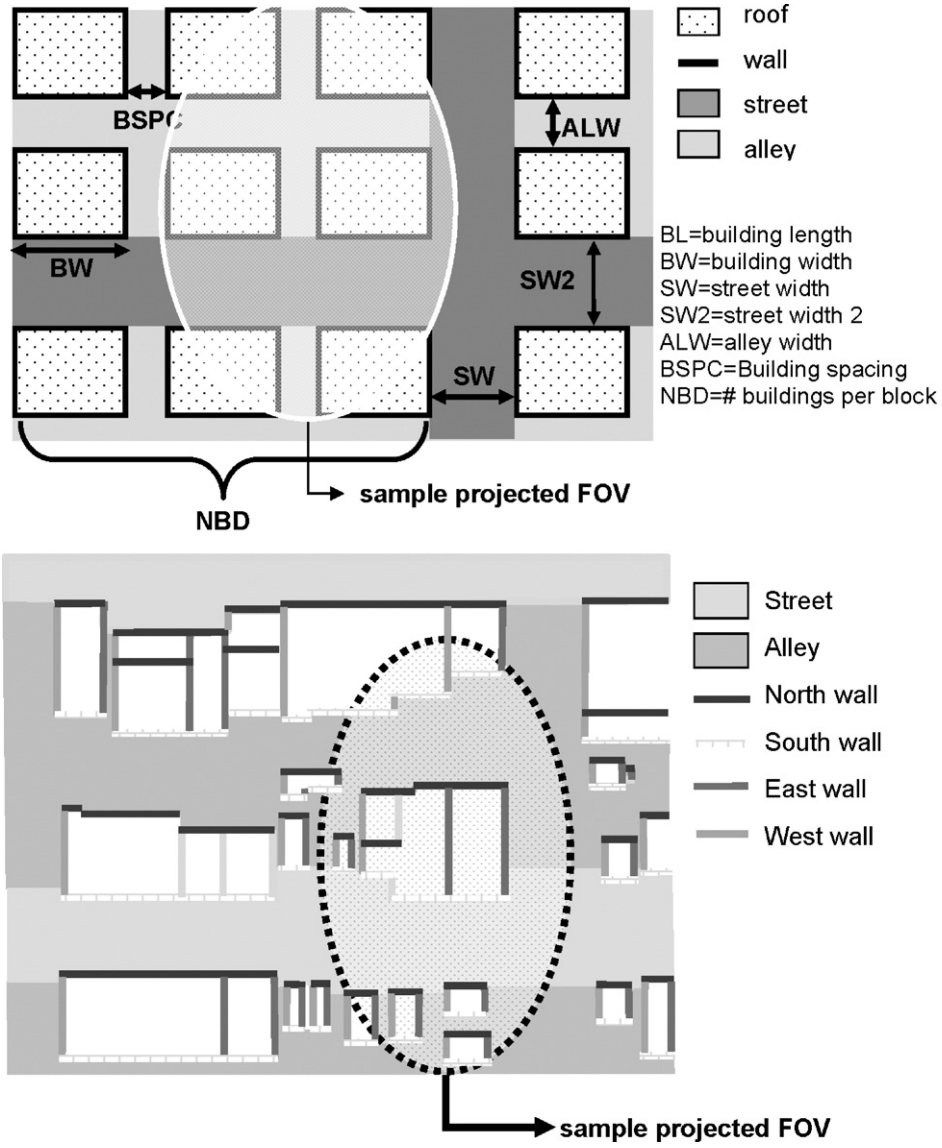

Fig. 1. Sensor IFOV projected onto a modeled urban surface using (Top) a simple surface representation, (bottom) GIS database for the light industrial study area.

The paper uses an updated version of the SUM model that includes a provision to incorporate a more realistic surface representation using individual building footprint data. The overall goal is to provide a first full-scale test of the ability of the model to estimate the thermal anisotropy at the urban land use scale, and demonstrate the applicability of the model to describing the full anisotropic behaviour of thermal radiation over select urban surfaces.

2. The SUM directional sensor view model

The SUM surface-sensor-sun relations model (Soux et al., 2004) represents how a remote thermal sensor views an urban surface. The remote sensor is specified in terms of instantaneous field of view (IFOV), and angular and azimuthal viewing geometry (all given in degrees) as well as sensor height and relative position to the surface structure. The urban surface structure is represented as a four dimensional array, where the first 3 dimensions are the urban surface structure, and the fourth stores particular attributes of each cell of the surface. The urban surface is composed of roofs, walls, roads and alleyways, although there is no formal restriction on the number of surface components that may be represented.

The urban surface is represented here in two ways: a simple repeating arrangement of buildings and streets (simple surface), and through a spatial database (Geographic Information System — GIS) of actual building footprints and heights (GIS surface). The simple urban surface consists of a regularly repeating series of rectangular-shaped buildings of equal dimensions (including height) that is defined in terms of a building width, length, height, street width, alley width, inter-building spacing and a number of buildings along a "block" (Fig. 1a). In the original model formulation (Soux et al., 2004) there was no provision for an inter-building spacing. The GIS surface reads in the building footprints and heights from a spatial database so that the actual building layout is preserved and variable building heights are accommodated (Fig. 1b). In this implementation, building facets are assumed to be in one of four orientations 90° apart relative to the primary street azimuth, which can be set to any direction. Extension to variable wall azimuths is not limited by the model formulation.

For each cell, the model determines whether the cell is shaded or sunlit, and whether it is viewed based on the given sensor viewing geometry. View factors for each viewed cell are calculated using a contour integration approach, and then summed and reported as totals for the sunlit and shaded components of

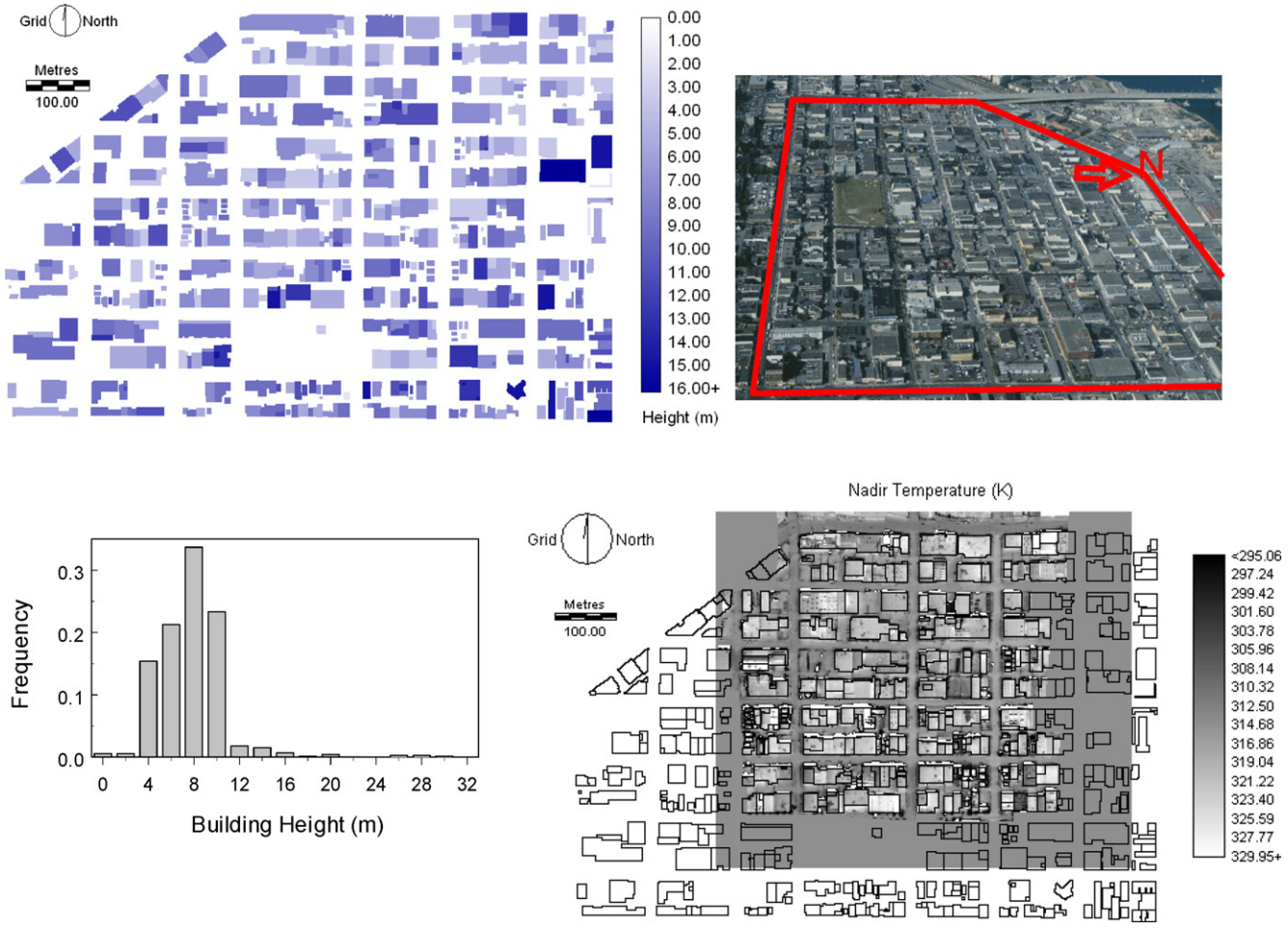

Fig. 2. Light industrial study area in Vancouver, BC. Canada showing: building GIS, site photo, building height frequency distribution and nadir thermal image composite overlaid with building footprints.

each facet of the urban surface. The view factors are then coupled with radiometric temperatures of the component surfaces to provide an estimate of the sensor directional radiometric (or brightness) temperature for a particular azimuth and viewing angle.

3. Data and methods

3.1. Building data

Surface databases of building footprints for two study areas: a light industrial (LI) area and a downtown (DT) area of Vancouver BC Canada (Figs. 2 and 3) were constructed. Building footprints in the LI study area were digitized from 1994 1:2000 scale aerial photos and confirmed with photos taken during the observation period. Building heights were estimated from field observations using an inclinometer in August 1994. Building footprints and heights in the DT area were taken from the 1984 City of Vancouver Planning Department Downtown Peninsula Map and updated based on the 1994 aerial photos, along with photos taken during the observation period. Building heights along the main traverse routes of the vehicle-mounted infrared thermometer array (Section 3.2) were updated from ground-based inclinometer measurements made within a year of the observation period.

The LI area is characterized by relatively long rectangular buildings of 3–4 stories with flat roofs, and largely devoid of vegetation (<5% Masson et al., 2002). The DT area is characterized by a few very tall massive buildings mixed in with a high density of lower (4–6 storey) buildings, again with very low amounts of vegetation. General characteristics of the sites are shown in Table 1. The digitized vector polygons were converted to a 1 m raster grid and coded as roofs, streets, alleys, building interior or one of 4 wall orientations. The scale of the downtown surface model was reduced by a factor of 3 (an individual cell array represents $3\times3\times3$ m) to reduce the array size in the SUM simulations. The building footprints replicate the configuration of the buildings, including representation of adjoining walls of equal heights that are a common feature in the LI area. A limited number of smaller scale building features such as elevator shaft housings are included where they formed a significant feature of the building roof in the LI study area, but in general, the fine-scale details of the buildings such as balconies, roof parapets, variable height roofs are not included.

3.2. Temperature data

Temperature data is required for two purposes: to provide input component surface temperature estimates for the modeled urban surface and to provide a validation data set for the SUM output. Radiometric temperatures were measured using two systems: an airborne thermal scanner and a ground-based array of infrared thermometers.

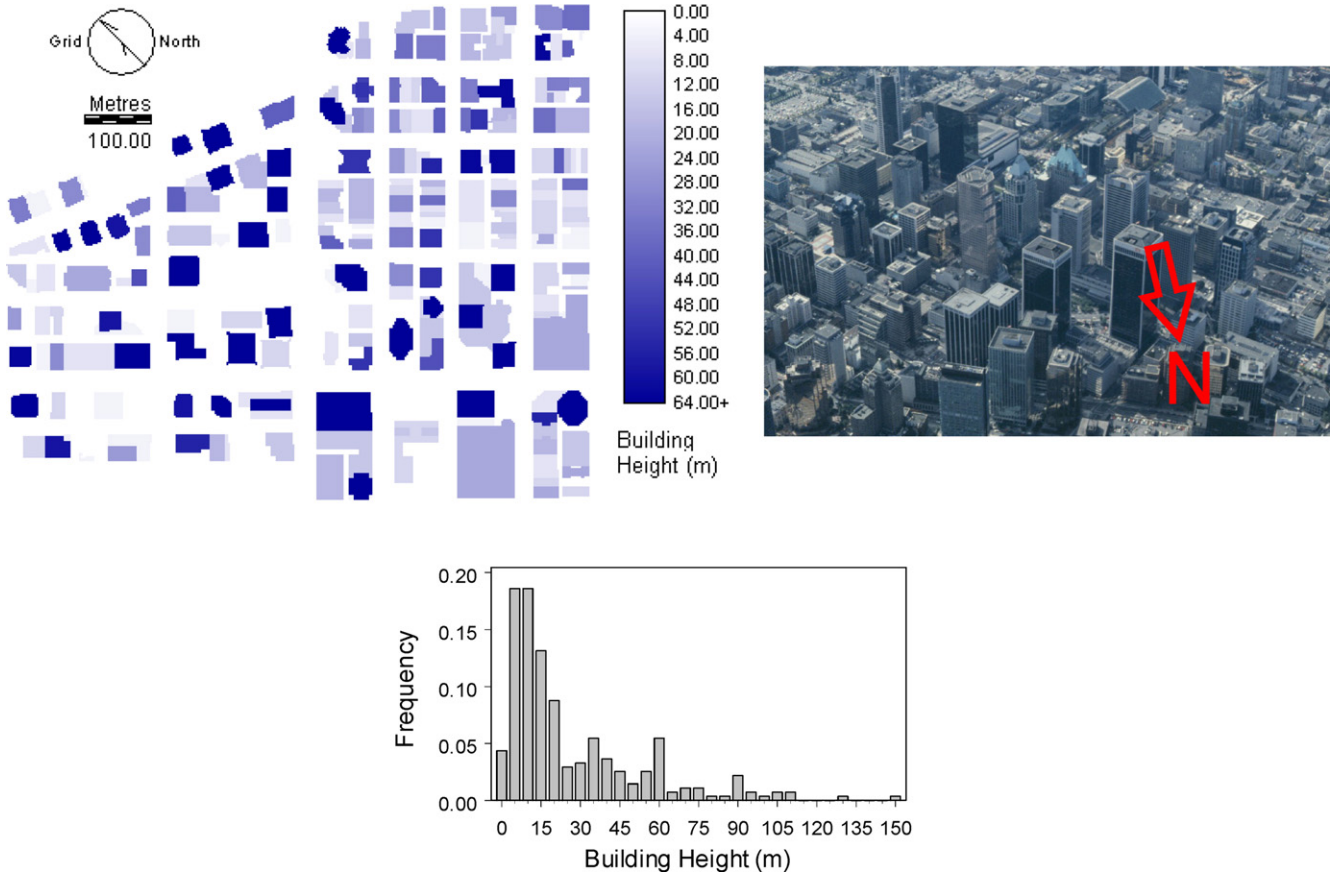

Fig. 3. Downtown study area in Vancouver BC Canada showing: building GIS, site photo and building height frequency distribution.

Table 1
Characteristics of the study sites and general observing parameters

Study site	Light Industrial	Downtown
Code	LI	DT
Building height	Avg. 7.3 m	Avg. 27 m; median 15 m
A_c/A_p	1.4	2.2
A_r/A_p	0.38	0.37
Date	15 Aug 92, YD 228	16 Aug 92, YD 229
Flight altitude: nadir (m)	647 m	689 m
Flight altitude: off-nadir	457 m	488 m
Number of flights	3	2
Off-nadir view directions	N, S, E, W	NW, SE, NE, SW
Flight Times (LST) Ground-traverse	Flight 1: 0900–1000 Traverse 228.4 0925–0949 Flight 2: 1245–1330 Traverse 228.7 1255–1318 Flight 3 1605–1645 Traverse 228.11 1630–1651	Flight 4 1015–1110 Traverse 229.5 1030–1107 Flight 5 1505–1545 Traverse 229.10 1509–1605
Solar Geometry (zenith/azimuth angles)	F1 48.9–45/121.5–129.9 F2 36.8–37.9/200.2–206.8 F3 61.3–64.2/257.4–261.1	F4 41.3–38.9/140.8–150.3 F5 51.2–54/241.7–246.3

The airborne thermal scanner (AGEMA 880 LWB) was equipped with a 12° field of view lens and was deployed from a helicopter. Images were sampled along flight lines using both nadir and 45° off-nadir viewing angles at azimuths orthogonal to each of the four major street orientations (Voogt & Oke, 1998a). A circular area on each image equivalent to a conical 12° field of view was extracted for comparison with modeled results (Fig. 4). A summary of the flights performed is shown in Table 1.

The ground-based array of non-scanning infrared thermometers was mounted on a vehicle that was traversed along all the streets and alleyways in the study area. Thirteen traverses were conducted on each of the two observation days, with traverses set to coincide with times of the overflights (Table 1). Sampling of road and wall surface temperatures was conducted at ~5 m intervals and the data was processed to remove observations from non-building surfaces and to identify the mean values of temperature distributions related to sunlit and shaded components of wall and road surfaces. Full details of the method are available in Voogt and Oke (1998b).

3.3. Methods

3.3.1. Viewing the surface

3.3.1.1. GIS surface. The position of the modeled sensor IFOV projected on the GIS surface (Fig. 1) was set to reproduce the observed position (as shown by the thermal infrared imagery) for both the start and end points of the flight line. Between these two points the modeled sensor position is incremented in equal steps across the GIS domain. Where significant differences in sensor viewing angle or azimuth occur along the flight line, the simulation is broken into sections, with separate viewing geometries for each section. At each sampling location the SUM model output (view factors for each sunlit and shaded surface component) is saved.

3.3.1.2. Simple surface. The urban surface parameters are chosen to best approximate observed dimensions of the area as derived from GIS analyses, and to preserve the non-dimensional complete to plan area ratio (A_c/A_p), and roof to plan area ratio (A_r/A_p). The SUM model is then run to sample the position of the projected IFOV on the surface across one full wavelength of the surface structure in both the x and y directions with the results saved for each sampling location.

3.3.2. Assigning surface temperatures

To estimate the sensor directional radiometric temperature, the calculated view factors are combined with radiometric temperature information for each surface derived from one of the methods described below. Temperatures are converted to equivalent 8–14 μm radiation during the summation using the method of Verhoef et al. (1997).

3.3.2.1. Facet average method. The facet average method of specifying facet temperatures results in a single temperature for each surface component (e.g. sunlit road, shaded road, sunlit east wall, shaded, east wall, etc.) Wall temperatures are derived from mean vehicle traverse data while roof and ground surface temperatures are derived from a separate set of thermal images taken from a nadir viewing angle and merged into a single composite image (Voogt & Grimmond, 2000). The GIS database is then used to extract mean temperatures of building roofs and ground (primarily road) surfaces. An adjustment for warming and cooling of roof surface temperatures between the time of the nadir flight lines and off-nadir lines is made for the morning and late afternoon flights over the LI area. The adjustment is based on the time series of roof surface temperature made by a single infrared thermometer mounted on one of the study buildings (see Masson et al., 2002).

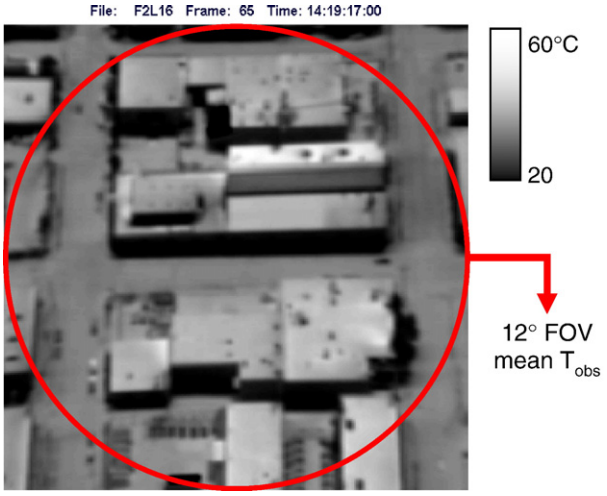

Fig. 4. Off-nadir thermal image acquired over the LI study area. The circle indicates the limits of the modeled conical IFOV.

Table 2
Horizontal surface temperature components for an early afternoon flight over the Light Industrial study area derived from analysis of the nadir thermal image composite

Surface	Roof		Road		Road (sunlit)		Road (shaded)	
	$\overline{T}$	σ	$\overline{T}$	σ	$\overline{T}$	σ	$\overline{T}$	σ
No filter	318.87	6.51	311.05	7.14	314.00	3.68	298.89	4.67
3×3	319.46	6.12	311.20	6.99	313.97	3.54	298.76	4.74
5×5	319.69	5.99	311.66	6.56	313.98	3.42	298.93	4.81
7×7	319.78	5.93	312.21	5.93	314.00	3.29	299.37	4.75

Separation of shaded and sunlit road surfaces is accomplished by inspection of the image histogram. Separation could be accomplished using a shading routine coupled with the GIS, but tests using Flight 2 showed that the shaded area determined in this manner was under-represented, in part due to the lack of representation in the GIS by small scale structures. The binary building "mask" image was filtered with different filter sizes (Table 2) to assess variability arising from inaccuracies in the match between the thermal image composite and the GIS building footprint. Following filtering, the images were reclassified so that all non-integer pixels were set to 0, thereby reducing the size of the defined surface. The difference between filtered and non-filtered surfaces is largest for roof surfaces and is minor for road surfaces. The relatively large change in shaded road temperature may be due to the filter size beginning to exceed the size of most shaded areas, which is relatively small at this time of day. Additional filtering of the roof mask shows decreasing variability of temperature (reduced edge effects) as filter size grows, and a decrease in the temperature change as filter size increases, indicating a greater likelihood that the mask incorporates only roofs. Based on this analysis, 3×3 filtered results are used for horizontal surfaces.

3.3.2.2. Multiple facet average method. The multiple facet average method was used for some model tests in the Light Industrial study area. It is similar to the facet average method except that in place of a single average temperature for each facet, a distribution of facet averages is created. For wall surfaces, vehicle traverse results are averaged for each street in the study area, yielding 11 averages for north and south walls and 5 averages for east and west walls. Averages for horizontal surface components were derived from a series of operations based on the nadir thermal composite image and the GIS surface. First, a mask of the component of interest (roof, sunlit ground, shaded ground) was multiplied by the nadir thermal composite image and unmasked areas assigned the mean temperature of the mask component. This image was then processed with a 155×155 filter to yield an approximate mean temperature for the component at a scale representing the projected IFOV of the airborne sensor. Finally, the filtered image was sampled with a regular rectangular grid and masked for edge effects to yield 572 sample points.

3.3.2.3. Image sampling method. Component surface temperatures were also determined by detailed sampling of images along each off-nadir flight line of the early afternoon flight over the LI area for comparison with the facet average method. Images were selected to give complete coverage of the flight line within the bounds of the observed images. Images selected were not included as part of the observed database. All roof, sunlit road, shaded road and wall surfaces that could be identified within a given domain for each image were digitized and the mean, standard deviation and area were saved. Digitized areas were corrected for "double-counted pixels" that sometimes occurred due to digitizing inaccuracy and/or the vector to raster conversion process. Using the individual statistics for each sampled image, a mean weighted temperature for each component of each flight line was calculated.

The difference between the domain area and all the digitized component surfaces is the residual area. The residual temperature associated with this area typically represents vegetated areas, partially sunlit areas, low emissivity areas, or other areas that could not be precisely identified. The residual temperature was used to modify the area-weighted sunlit road and shaded ground temperatures using (all symbols defined in the Glossary)

$$T_{\mathrm{rd}} = [A_{\mathrm{rd}}T_{\mathrm{rd}} + F_{\mathrm{rd}}(T_{\mathrm{res}}A_{\mathrm{res}})]/(A_{\mathrm{rd}} + A_{\mathrm{res}}F_{\mathrm{rd}}) \quad (1)$$

$$T_{\mathrm{shd}} = [A_{\mathrm{shd}}T_{\mathrm{shd}} + F_{\mathrm{shd}}(T_{\mathrm{res}}A_{\mathrm{res}})]/(A_{\mathrm{shd}} + A_{\mathrm{res}}F_{\mathrm{shd}}) \quad (2)$$

This modification essentially apportions the non-sampled (residual temperature) to the horizontal surfaces (sunlit road and shaded area). The existing SUM surface component categories then better represent the entire ground surface temperature distribution; an alternative approach would be to provide more

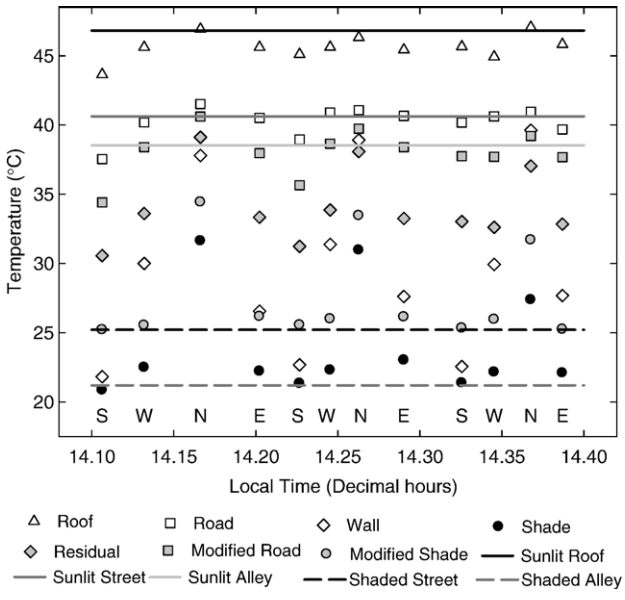

Fig. 5. Component surface temperatures for the off-nadir flight lines of the early afternoon flight over the LI area. Symbols represent mean values derived from detailed sampling of individual images for each flight line with a view direction as indicated near the bottom of the image. Lines represent the single mean temperature from the facet average method for roofs, and sunlit and shaded components of streets and alleyways. Modified road and shade temperatures incorporate the residual image area.

categories of ground surface components (e.g. surface vegetation, gravel, sidewalks etc.) within SUM.

The results of the facet average and detailed sampling methods are shown in Fig. 5 and may be summarized as:

- roof temperatures are well approximated by the use of the facet average method;
- when differentiated in the facet average method, alleys are cooler than streets for both sunlit and shaded components;
- modifications to road and shaded temperature components (Road(m), Shade(m)) using the residual temperature cool the road and warm the shaded component (Fig. 5);
- sunlit wall temperatures derived from image sampling are warmer than those observed from the truck-mounted infrared thermometers;
- view directions to the north have relatively warm shaded surfaces but these form a very small fraction of the field of view and do not strongly impact the results (0.15 °C difference in modeled temperature for a 5 °C change in shaded surface component temperature).

4. SUM model evaluation

The SUM model evaluation is carried out using the GIS surface viewing method and the facet average method for specifying the component surface temperatures. The modeled radiometric temperature is then compared to the mean temperature from the images, derived from a circular portion of the image (Fig. 4) to coincide with the SUM sensor projected IFOV. All the simulations for each flight line are averaged and compared to the mean temperature of the images for that flight line, and model validation statistics are calculated on the basis of these averages.

4.1. Light Industrial area

Results of the model comparison for the Light Industrial area (Fig. 6), suggest a tendency for a slope <1; i.e. an overestimation for view directions where more shaded surfaces are seen e.g. southerly and easterly view directions for the morning flight, southerly view direction for the early afternoon flight and an underestimation for view directions that include the most strongly sunlit facets. The southerly view direction for the early afternoon flight in particular is characterized by a substantial overestimation, and this is reflected in the poor statistical validation measures (Table 3). Together, these deficiencies result in a substantial underestimate of the overall thermal anisotropy of the surface — as expressed by the range of the modeled versus observed values. The variability of the observed temperatures, represented by averages of different flight lines and their associated standard deviations (error bars) is larger than that of the modeled results, indicating the importance of temperature variability for surface components relative to the variation in surface structure alone. During the morning and late afternoon flights, some temporal variation of surface temperatures between flight lines is expected (e.g. as shown in Fig. 5) and may account for some of the variability in the observed temperatures.

Table 3
Validation statistics for each of the overflights

Flight	Flt 1	Flt 2	Flt 2*	Flt 3	Flt 4	Flt 5
Area	LI	LI		LI	DT	DT
Time (LST)	0930	1300		1630	1100	1530
Statistic						
b (slope)	0.33	0.35	0.9	0.53	0.77	0.80
a (intercept)	21.3	26.7	4.0	16.1	6.9	6.0
RMSE (Root Mean Square Error)	1.34	1.71	0.38	0.67	1.52	1.09
RMSEs (Root Mean Square Error systematic)	1.31	1.69	0.22	0.64	1.20	0.69
RMSEu (Root Mean Square Error unsystematic)	0.26	0.25	0.31	0.19	0.94	0.84
MBE (Mean Bias Error)	0.16	0.97	−0.04	0.14	0.66	0.37
MAE (Mean Absolute Error)	1.22	1.37	0.31	0.58	1.24	0.93
d (Index of Agreement)	0.74	0.70	0.99	0.90	0.96	0.96

Model results obtained using the GIS surface viewing method and facet average method for assigning surface temperatures. Flt 2* represents statistics calculated using detailed sampling of image component temperatures.

Fig. 7 compares the modeled versus observed directional temperature of the early afternoon flight over the LI area using both the image sampling method and facet average method for providing component surface temperatures. A substantial improvement in statistical agreement is achieved for all parameters (Table 3). The improvement comes about through large changes in the modeled temperatures for the south view direction and also to some extent for the north view direction. A comparison

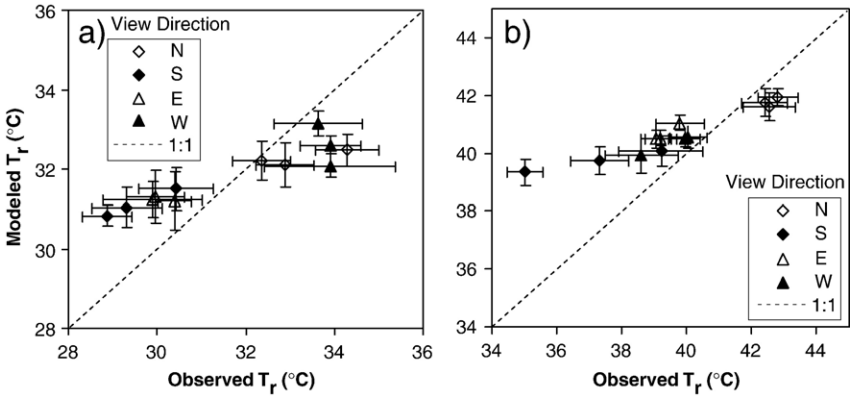

Fig. 6. Comparison of observed and modeled directional radiometric temperatures of four 45° off-nadir viewing directions for the a) 0930 LST and b) 1300 LST flights over the Light Industrial area.

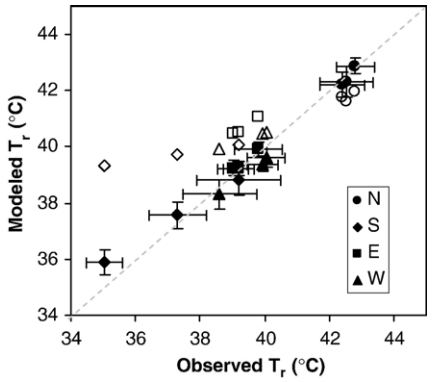

Fig. 7. Comparison of observed and modeled directional radiometric temperatures of four 45° off-nadir viewing directions for the early afternoon flight (1300 LST) over the Light Industrial area using both the image sampling method (solid symbols) and facet average method (open symbols) to determine component surface temperatures.

of the component surface temperatures (Fig. 5), as well as the average view factor for each component, shows that for the south view direction, the improvement in modeled values is derived largely as a result of the variability of sunlit road and roof temperatures, especially a decrease in these values for two flight lines relative to the mean values used in the standard approach. For the north view direction, the most significant differences are due to underestimation of the south-facing wall temperature and alley temperatures by the standard method, whereas for the east view direction, sunlit street, roof and wall temperatures are approximately equally responsible. This assessment suggests the original differentiation of the streets from alleys is not particularly important relative to the provision of surface temperatures for non-road surfaces (the inclusion of the "residual" temperature). Some variability in roof temperature, especially a consistent difference between south and north viewing directions, may be related to shading by microscale roof surface structures within the sampled roof area.

4.2. Downtown area

A comparison of modeled and observed directional radiometric temperatures over the downtown study area show relatively good agreement (Fig. 8, Table 3). There is a tendency, as for the LI area, for the warmest temperatures to be underestimated and the coolest temperatures overestimated, however the effect is more muted than in the LI area. Use of the simple urban surface structure that approximates A_c/A_p and A_r/A_p yields similar results, but with a greater tendency to overestimate cool temperatures and underestimate the warmest directional temperatures (results not shown). The spatial variability of results is much reduced through the use of the regular urban surface structure.

4.3. Summary

It is clear from the model evaluation that the modeled results are highly sensitive to specified input facet temperatures. Three specific factors related to the input temperature were found to be important. First, temperatures of the sunlit walls as derived from analysis of the thermal imagery are warmer than those estimated by the ground-based truck traverses. This is likely related to the ground-based sampling of surfaces deeper (and more likely to be shaded) within the street canyons, and which may also be affected by reflection of cold sky radiance from low emissivity building surfaces. These temperatures may be correct for the viewing position, but may be hidden from airborne view by awnings or other small scale surface features that are not incorporated in the SUM model surface representation. Thus, use of surface temperatures derived from vehicle-mounted instruments in the SUM model may impart a low temperature bias, especially for the most sunlit walls. Second, the temperature distributions on streets of different orientations can be quite different. SUM at present does not account for street orientation, however the shading history of a surface can substantially modify the modal values for sunlit and shaded components of the surface; use of an average value leads to poorer agreement. Third, the specification of "alley" surfaces for the downtown area is confined to the very narrow streets and courtyards between buildings, and forms a relatively small proportion of the overall area. The sunlit temperature component of these surfaces is likely to be cooler due to a shorter warming period because of greater shading in these confined areas.

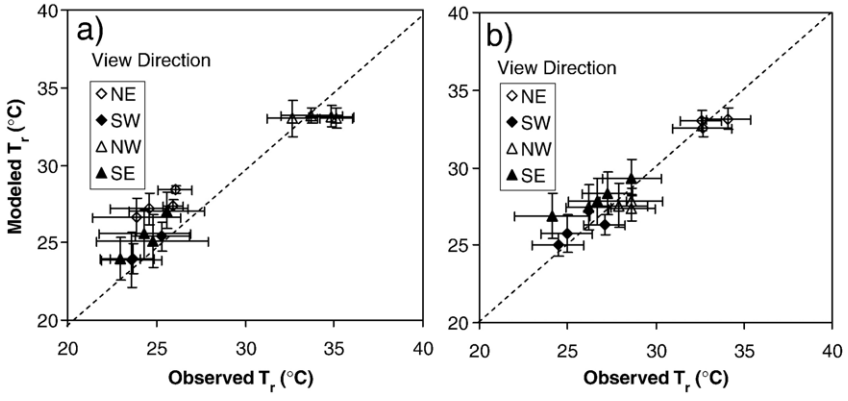

Fig. 8. Comparison of modeled and observed directional radiometric temperature of four 45° off-nadir viewing directions for the downtown study area a) at 1100 LST (Flight 4) and b) 1530 LST (Flight 5). Model results use the GIS surface and facet average temperature methods.

Table 4
Model sensitivity simulations of sensor-detected temperature

Simulation name	Surface geometry	Surface temperature method
Fixed urban surface	Simple surface	Facet average
GIS surface	GIS surface	Facet average
T variation only	GIS surface [a]	Multiple facet average [b]
Combined	GIS surface [c]	Image sampling [d]

Notes:
All tests performed using data from the early afternoon flight over the Light Industrial area.
[a] The view factors for each component are averaged for all sampling locations.
[b] Samples are combined with mean view factors to yield 11 × 572 modeled temperatures for north and south view directions and 5 × 572 temperatures for east and west view directions (see Section 3.3.2 for details).
[c] View factor calculations are performed at 36–57 sensor positions for east and west view directions, 41–80 for north–south view directions to coincide with airborne observations.
[d] Between 4–7 images per flight line are sampled, each generating a set of facet temperature averages.

In order to further assess the sensitivity of the modeled anisotropy to input surface conditions a number of sensitivity tests were conducted to identify the contribution of variations in surface structure and surface temperature to the urban thermal anisotropy. These are discussed next.

5. Sensitivity analysis

5.1. Sensitivity to surface structure and temperature

The sensitivity of the modeled sensor temperature to both surface structure and surface temperature was examined by comparing the observed temperature distribution to four separate model simulations (Table 4). The first two simulations examine the effect of the two urban surface representations (GIS and simple surface) and use a fixed average temperature for each of the surface components. The third simulation keeps the surface geometry, as represented by the average view factor for each surface component, fixed and combines this with temperature variability for each of the surface components. The final simulation combines variable surface geometry using the GIS surface with temperature variations from the image sampling method for each surface.

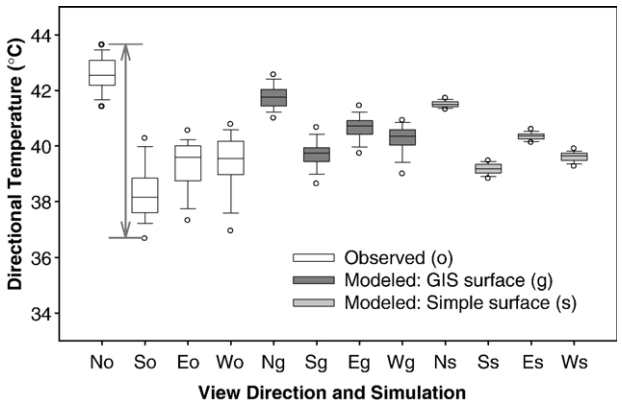

Fig. 9. Box plot of modeled directional temperature for the simple and GIS urban surface as well as the observed sensor temperature. Boxes represent the 25th, 50th, and 75th percentiles, error bars the 10th and 90th percentiles and symbols the 5th and 95th percentile. The arrow represents the range of temperatures equivalent to the anisotropy.

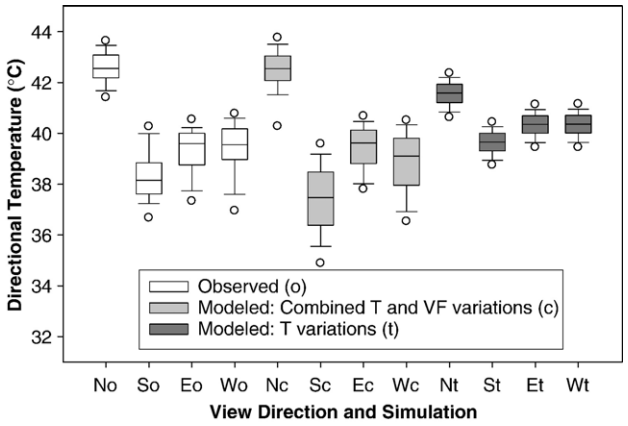

Fig. 10. Box plots of observed and modeled directional temperature. The plots labeled "T variations" use the mean view factor for each view direction derived from the GIS surface viewing method and combine this with variations in temperature across the LI study area obtained from the multiple facet average method. The combined modeled results use the image sampling method for specifying facet temperatures and combine these with all the modeled view factors along the flight line using the urban surface GIS (see Table 4 and Section 3.3.2 for details) Box plot parameters are as defined in Fig. 9.

Results, shown as box plots, are presented in Figs. 9 and 10. It is clear that the simple urban surface representation given by the internal SUM surface geometry provides relatively little variation and substantially underestimates the full anisotropy of the surface (shown by the superimposed vertical arrow). The use of the GIS surface increases the variability of the modeled temperature in each view direction but the overall anisotropy increase compared to the simple geometry is relatively small (mostly an increase in the maximum temperature for the north view direction). Compared to the observed temperature variability, the GIS surface accounts for approximately 60% of the total anisotropy. Facet temperature variability alone accounts for roughly the same amount of modeled temperature variability as the GIS surface structure (Fig. 10). The combined simulation, in which view factors derived from the surface GIS and variable facet surface temperatures from the image sampling method covary, shows variations of the same order, or in some cases larger, than the observed. The increase in variability here comes from the full combination of temperature with view factors — in reality not all surface structures would exhibit the full range of temperature variability tested. The simulations suggest that surface geometry and facet temperature variability (due to surface material variations) have roughly equal contributions to the overall observed temperature variability.

5.2. Sensitivity to omission of small scale surface structure

Another factor that may contribute to the deficiency in the validation of Fig. 6 is an underestimation of the shaded area viewed, possibly due to small scale surface structures that are not represented in either the simple urban surface or the GIS database. To determine if this interpretation has merit, a number

of additional tests were made. First, the summed view factors for all shaded components seen by the sensor was compared to the fraction of pixels from all images that fall below a threshold shaded/sunlit temperature value (Fig. 11). This test was performed for both morning and early afternoon flights over the LI area. The temperature contrast between shaded and non-shaded areas is greatest in the morning since the area that converts from sunlit to shaded is relatively small. If the total shaded view factor is less than the area of temperatures that correspond to shaded areas it may suggest that the images are characterized by more shade than is represented in the surface GIS. The effect would be maximized for view directions towards the solar azimuth. Inspection of Fig. 11a suggests that the total shaded view factors may be slightly low for the east and south view directions for Flight 1. Much smaller view factors (and fractions of shaded pixels) are noted for north and west view directions. Modeled view factor ranges are very small whereas the fractional area of temperatures less than the threshold is larger; this larger fraction incorporates variability in surface characteristics as well as surface structure. For the midday flight, the most apparent differences are from the west and east viewing directions (nearly orthogonal to the solar azimuth). The west

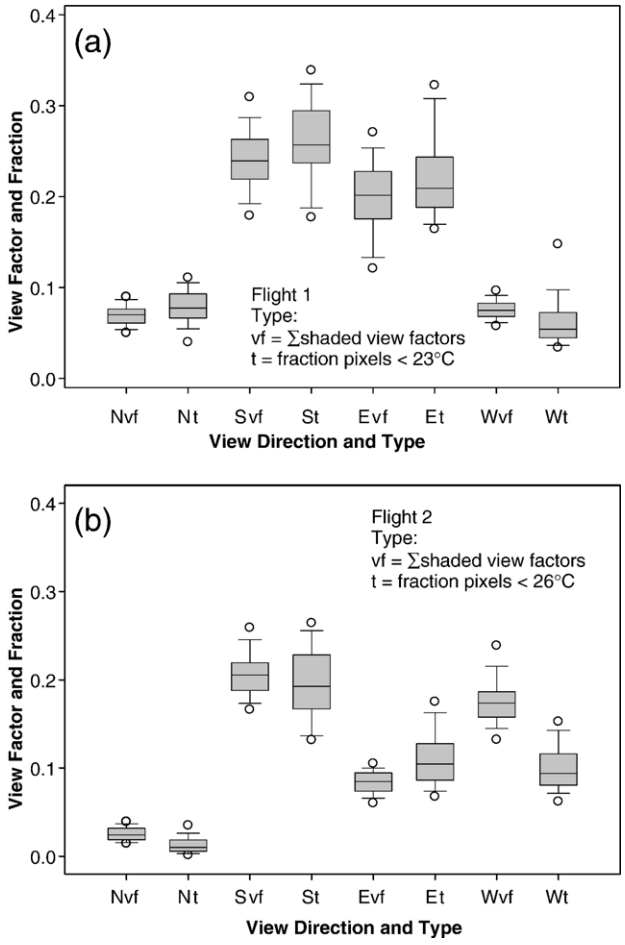

Fig. 11. Box plots for: (a) Flight 1 and (b) Flight 2 comparing the total view factor for shaded surfaces in each of the off-nadir viewing directions with the fraction of pixels within the projected IFOV that fall below a threshold that approximates the sunlit/shaded temperature boundary.

Table 5
Dimensions (m) of test surfaces used to assess the view factor of additional small roof structures (RS) to buildings (B)

Surface	H_B	H_{RS}	W_{RS}	L_{RS}	A_c/A_p	$A_{r(RS)}/A_{r(B)}$	$A_{c(RS)}/A_{c(B)}$
Buildings only[a]	7	–	–	–	1.428	–	–
Small RS	7	3	6	12	1.490	0.117	0.132
Medium RS	7	3	8	14	1.504	0.194	0.185
Large (RS)	7	3	10	16	1.518	0.302	0.248
Small RS, scaled by A_c	6	3	6	12	1.429	0.117	0.144
Large RS, scaled by A_c	6	2	10	16	1.427	0.302	0.226

Height, width and length of roof structure (H_{RS}, W_{RS}, L_{RS}) and height of building (H_B) for each simulation are specified as well as complete (A_c), plan (A_p) and roof (A_r) areas for both buildings and roofs structures.
Areas are calculated for one complete "wavelength" of the surface.
[a] Surface structure (all values in m): buildings 30×23, 3 buildings/block; streets 22, alleys 12, inter-building spacing 9.

view direction at this time is newly shaded, hence the relatively large modeled shaded view factor. However the temperature range remains large from the differential heating of surfaces with different radiative and thermal properties through the morning, so these newly shaded surfaces tend to exhibit a range of temperatures depending on their particular surface properties. The heating and cooling history of the surface thus tends to lower the fraction of pixels less than the fixed threshold. In contrast, the east view direction is towards newly sunlit walls, so the shaded view factor total is lower, but these surfaces have yet to warm significantly, so the fraction of "shaded" surfaces based on the threshold temperature remains large. There is little difference between the modeled shaded view factor and the fraction of cool surfaces for the south view direction for which relatively few pixels will have changed status from sunlit to shaded.

A second test used a regular surface geometry with the complete area (A_c) set to match that of the LI study site and then added small structures to the building roof. These structures represent elevator shaft housings or small penthouses that may not have been included in the original GIS. Three sizes of structures were tested (Table 5). The structures occupy between 12–30% of the plan roof area and 13–25% of the total building area (vertical and plan surfaces). Initial simulations simply added the roof structure to the base building structure leading to an increase in the overall complete surface area of the study domain. A second set of simulations was conducted with the largest and smallest of the roof structures in which the building height and/or roof structure height was adjusted to keep the complete surface area and A_c/A_p fraction approximately constant.

When roof structures are added (without attempting to preserve the complete surface area) the shaded view factor increases for view directions towards the Sun (Fig. 12a) compared to the no roof structure case. When the roof structure is added and the building height is adjusted so that A_c/A_p is preserved (Fig. 12b), only minor changes in the shaded view factor are noted (less than 0.01) and these are not likely to be significant. These results suggest that omission of small scale structures from the surface GIS is potentially important in cases where the base building structure is well represented (e.g. from

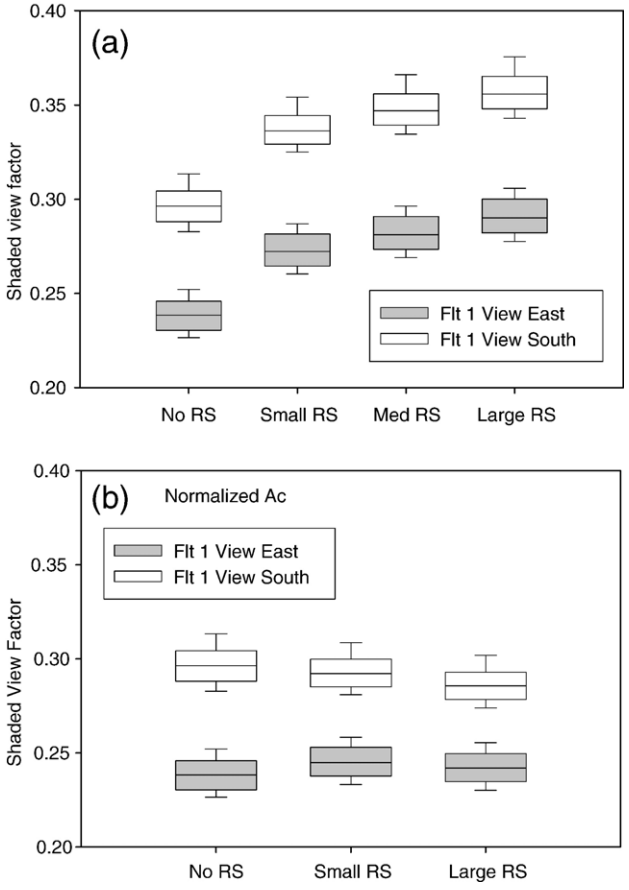

Fig. 12. Box plots of shaded view factors for select view directions of Flight 1 when additional roof structures (RS) are added to modeled buildings. (a) Simulations of three roof structure sizes added to buildings. (b) Simulations of the large and small roof structures where building heights are set so as to preserve the complete area for each simulation.

building footprint information) but when roof top structures are not included, and are a notable feature of the structures. If the building, omitting the actual roof top structure, has a similar complete surface area to that including the roof top structure, then the view factors are similar. However, this does not take into account the different relative position of shadows cast by a simplified building relative to that with a roof structure; in the former case, the shaded view factor of the main building wall and ground area is increased, in the latter, the shadow is projected first onto the roof, then at larger zenith angles onto the ground. The shading influence on the roof top versus ground surface may be important to anisotropy depending on the relative temperature differences involved.

A simple test using the internal SUM surface geometry was used to compare results between two model runs that used an identical surface layout (i.e. building footprint and building arrangement along the streets), but with different mean building heights, one set at the mean for the study area as derived from the GIS analysis (7 m) and the second set to (a somewhat arbitrary) 10 m. Altering only the building height preserves the plan area ratios of roof and ground area but increases the wall and complete areas. This scenario represents cases where the GIS captures the main urban surface structure, but misses features that have a small plan area and a relatively large vertical surface area which could cast significant shadows. Such features might include fences, hedges or utility poles. Using the same facet component temperatures for both simulations, the results (Fig. 13) show that the sensor observed temperatures are decreased most for view directions towards the solar azimuth (S and E directions). The difference in the direction most closely matching the solar azimuth (W) is very small. At this time of day there is also a relatively large change in the temperature for the north view direction due to the increase in shaded area of north–south streets. This change would be smaller as the solar azimuth approaches 180°. The changes illustrated in Fig. 13 would act to improve some, although not all, of the modeled-observed differences shown in Fig. 6. The results for actual small scale surface structures on the ground may be more muted as there is a chance they may exist within already existing shaded areas.

6. Sum model assessment for other viewing directions

The SUM model provides the ability to extend the analysis to other viewing angles and azimuths not sampled by the airborne scanning system. As a demonstration of this capability, model simulations are performed for the LI (early afternoon flight, Flight 2 — Table 3) and DT (late morning, Flight 4) study areas at 5 degree increments in off-nadir angle (up to 55°) and 10 degree increments of sensor azimuth.

The LI simulation takes into consideration the sensitivity analysis that shows the importance of representing both the surface structure and temperature variability by using the surface building GIS and coupling this with: a) for horizontal surface temperatures, the nadir thermal image composite of the study area at 1 m resolution, geo-referenced to the building GIS database (Fig. 2), and b) assigning wall temperatures to buildings such that the temperature frequency distribution

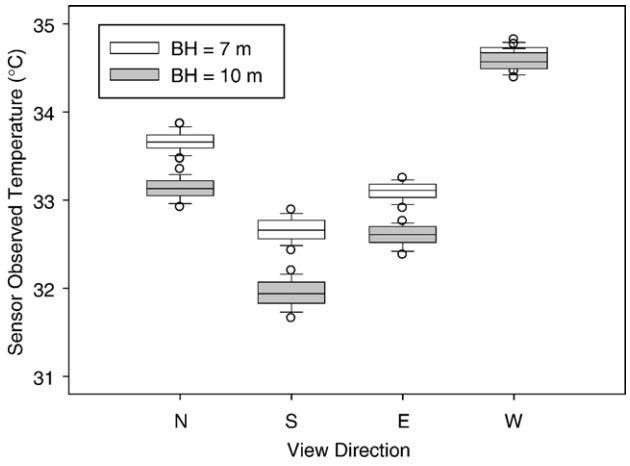

Fig. 13. Modeled sensor observed temperature using identical surface layouts for two different building heights. Variability of the modeled temperature comes from moving the sensor position such that the modeled IFOV is moved across the surface in 2 m increments.

observed by the vehicle traverses is preserved for each of the wall orientations. A separate frequency distribution is used for sunlit and shaded components of each wall, where necessary (south and west-facing walls at this time).

The domain that contains the modeled sensor IFOV is a 350 m × 350 m square with the sensor position adjusted so that the IFOV is centred on the middle of the domain for all viewing angles. The horizontal area of the sensor IFOV varies from approximately 7×10^3 m^2 for a nadir view (~95 m diameter) to 27×10^3 m^2 (an ellipse with length 233 m and width 148 m) at 50° off-nadir angle for the specified 450 m observing height. Seventy different domain positions were tested within the area that includes the composite nadir temperature image.

To summarize the results, statistics for each sensor view direction (each off-nadir angle and azimuth presented in the polar plot) were calculated (Fig. 14). The polar plots include interpolation of results in both viewing angle and direction (3 intermediate points) to increase the resolution of plotted points. The mean temperature (Fig. 14a) smoothes the variability of the individual polar plots and shows a hot spot for viewing azimuths centred around the northerly viewing direction and decreasing gradually as azimuths increase or decrease towards the east and west respectively. Nadir viewing directions remain relatively warm, not surprising for this time of day with peak roof and road temperatures, and a relatively open canyon geometry. The coolest temperatures are for large off-nadir viewing angles in the direction of the solar azimuth that view the largest shaded areas (projected onto streets in a north and slightly eastern direction at this time). Large off-nadir viewing angles in southeasterly azimuths are also very cool, and cooler than those in a direct southerly direction. The increase for the southerly direction is likely related to the north–south streets which are very warm at this time of day. A comparison with the results of Lagouarde et al. (2004) show a smaller variation of temperature across the polar plot and a tendency for the nadir viewing direction to be close to the warmest view direction. These findings are in agreement with the expectation of Lagouarde et al. (2004) for less dependency of the anisotropy on canyon geometry and more on individual surface material characteristics for land use types such as the LI study area where building heights and canyon height to width ratios are relatively low. The smoothness of the polar plots represents the averaging that occurs over the projected IFOV. The ground resolution of the current simulations is much larger compared to the 6.6–16.2 m resolution for nadir and 50° off-nadir angles used in Lagouarde et al. (2004).

The standard deviation for each view direction (Fig. 14b) tends to be largely symmetrical about the nadir point as is the range image (Fig. 14c). This effect is due to the relatively small size of the projected IFOV for the nadir view direction relative to the off-nadir viewing angles and the sensitivity of the modeled temperature to the exact positioning of the IFOV on the surface, where it may be easily dominated by one surface type with (e.g. sunlit rooftop or sunlit or shaded street). Interestingly, the nadir standard deviation is very similar to that obtained by Lagouarde et al. (2004) who report an average standard deviation of nadir temperature of 1.2 °C for their city centre site in Marseille. The

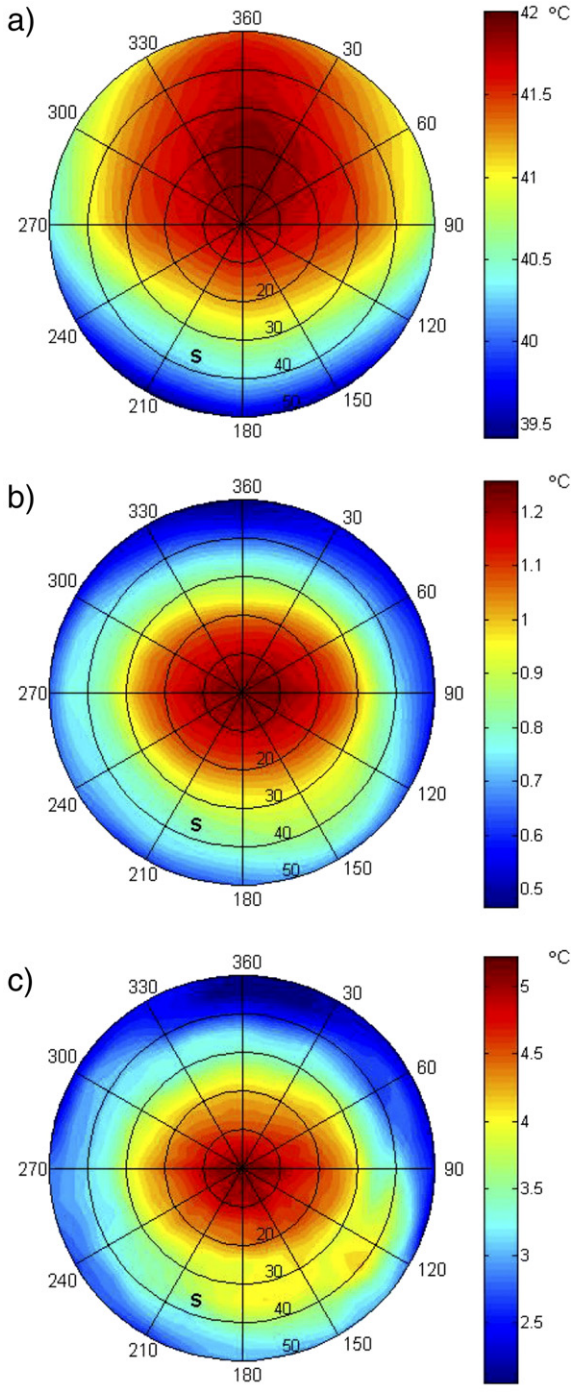

Fig. 14. Statistics for the modeled directional radiometric temperature (°C) over the Light Industrial study area (early afternoon flight) for each viewing direction (5° increments in off-nadir angle and 10° increments of azimuth angle) shown as polar plots. a) Mean value for each viewing position, b) standard deviation, c) range. **S** indicates the position of the Sun.

smallest variability is noted for large off-nadir view angles towards the north where a maximum view of warm south-facing walls that have the largest range of temperatures represented in the wall temperature frequency distribution.

The simulation for the downtown area uses mean facet temperatures coupled with the building GIS. Off-nadir angles

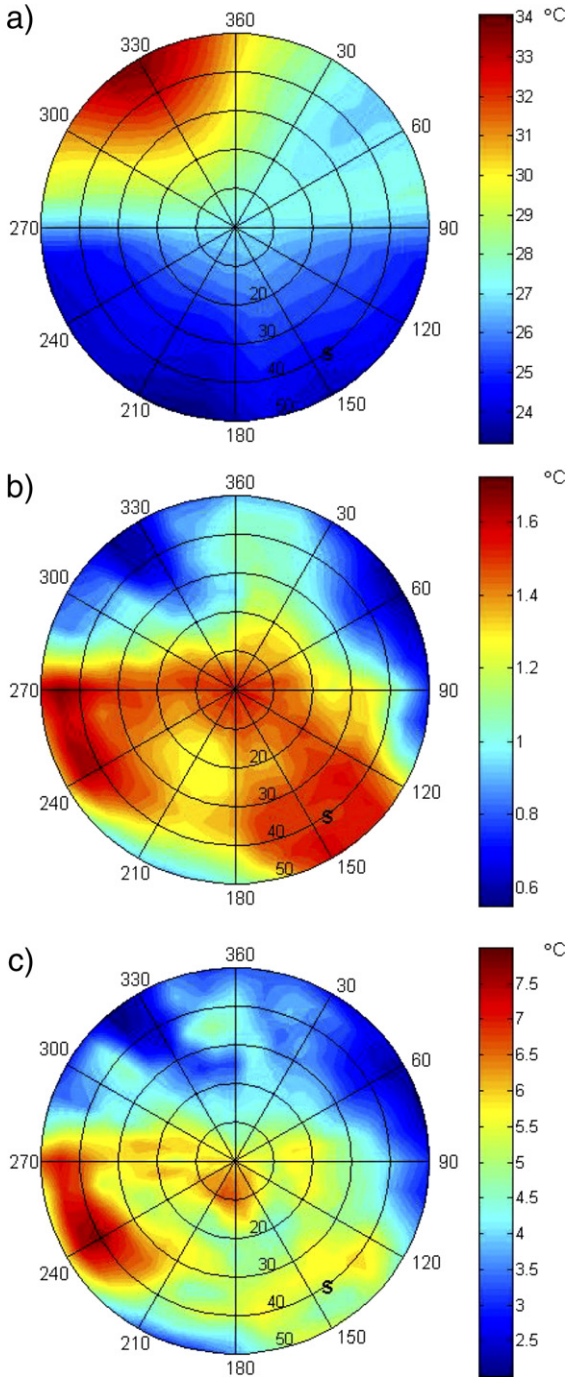

Fig. 15. Same as Fig. 14 except for 31 positions over the Downtown study area using data coinciding with Flight 4 (Table 3). Note the street orientation is aligned at 45–225°/135–315°.

are restricted to 50° to allow a slightly smaller domain for sampling within the GIS building domain. Results (Fig. 15) are based on 31 separate sampling positions of the modeling domain, with separations of 90 m to provide full coverage of the GIS domain and reduce overlap between neighbouring sampling positions. Anisotropy is ~10 °C, much larger than for the LI area and in line with observations (Voogt & Oke, 1998a). The warmest temperatures are observed when viewing towards the NW, in accordance with the most-directly sunlit walls at this time (nearly directly opposite the solar azimuth) and noting the orientation of the streets that are aligned NE-SW and NW-SE in this study area (Fig. 3). The coolest temperatures are offset towards the south and southwest, rather than directly towards the solar azimuth. Given the near coincidence of the solar azimuth with the street orientation at this time, views along the NW-SE roads in the direction of the solar azimuth may include the relatively warm sunlit streets at this time, but viewing azimuths slightly more towards the south and west will more likely include the shaded sides of buildings. The asymmetry between temperatures observed at view angles orthogonal to the solar azimuth likely indicates the warming of walls with a south-westerly orientation at this time. Nadir view temperatures are intermediate between the warm and cold extremes at higher off-nadir angles. This effect represents the larger role of walls in the directional temperature and the narrower canyon geometry that reduces the ground-level temperatures compared to that of the roofs. The patterns of variability expressed by the standard deviation (Fig. 15b) and range (Fig. 15c) are more complex than those of the LI area and are likely affected by the particular configuration of buildings, especially large tall buildings and open areas, within the study domain. Standard deviations for large off-nadir view angles in the direction of the most sunlit-facets (330, 60°) are low (and perhaps lower than if some measure of wall temperature variability had been included); in the opposite directions, variability increases presumably due to shading patterns and is spread from nadir to large off-nadir viewing angles.

Overall, these simulations confirm that the limited view direction sampling (nadir plus orthogonal to the road network pattern at 45° off-nadir view angle) used to obtain the airborne observations of Voogt and Oke (1998a,b) should incorporate the majority of the anisotropic temperature range.

7. Summary

The SUM model can generate reasonable estimates of the directional radiometric temperature, but results are highly dependent on the ability to provide appropriate facet temperatures and the specification of these temperatures can be difficult. The model results for both study areas suggest some consistent biases that lead to the underestimation of the effective anisotropy for the surface compared to observed values. The effect is more evident in the Light Industrial study area. Extension of results, using the SUM model, to full hemispheric plots, shows spatial variability for the tested sensor specifications, but when composited over a number of positions in the study area, the averaged results by view direction are smoothly varying and in accordance with expectations for the given surface structure and solar position.

The use of actual surface structure from GIS data improves the model's ability to capture the spatial variability related to the thermal anisotropy compared to the use of the SUM model's regular internal urban structure, but this variability is still reduced relative to that from observations due to the use of mean temperature values for all the modeled surface facets.

Detailed analysis and sensitivity testing for one study area shows that representation of the microscale temperature variability of the surfaces is needed for the model to correctly represent the full anisotropy of the surface. This finding is in agreement with the expectations of Lagouarde et al. (2004) who noted that a range of surface material characteristics and more open canyon geometry make the individual surface characteristics relatively more important in determining the overall thermal anisotropy of such areas, compared to those of urban or residential land uses. An important implication of this finding is that the specification of surface temperatures, for example from model output, must include microscale variability, and not simply represent facet averages, if the full range of anisotropy is to be represented. At present, most urban surface energy balance models that can be used to estimate urban surface temperatures for use in assessing anisotropy with a view direction model such as SUM provide only facet averages of temperatures based on mean thermal and radiative surface characteristics.

The application of the SUM model is limited by the need to have detailed observations of the radiometric temperatures of all component surfaces. Work on coupling SUM to a three-dimensional surface energy balance model (Krayenhoff & Voogt, 2007) that is capable of representing the full microscale variability of urban surface temperatures is underway and some initial tests have been conducted (Voogt & Krayenhoff, 2005).

Acknowledgements

This research was supported by funding from the Natural Sciences and Engineering Research Council of Canada. Thanks are due to E.S. Krayenhoff, A. Soux and M. Van De Wiel for discussions on model development and to J-P. Lagouarde, D. Aldred and E.S. Krayenhoff for assistance with developing routines for the polar plots.

References

Iino, A., & Hoyano, A. (1996). Development of a method to predict the heat island potential using remote sensing and GIS data. *Energy and Buildings*, *23*, 199–205.

Krayenhoff, E. S., & Voogt, J. A. (2007). A micro-scale 3-D urban energy balance model for studying surface temperatures. *Boundary-Layer Meteorology*, *123*, 433–461.

Lagouarde, J-P., Moreau, P., Irvine, M., Bonnefond, J-M., Voogt, J. A., & Solliec, F. (2004). Airborne experimental measurements of the angular variations in surface temperature over urban areas: Case study of Marseille (France). *Remote Sensing of Environment*, *93*, 443–462.

Masson, V., Grimmond, C. S. B., & Oke, T. R. (2002). Evaluation of the town energy balance (TEB) scheme with direct measurements from dry districts in two cities. *Journal of Applied Meteorology*, *41*, 1011–1026.

Nichol, J. E. (1998). Visualisation of urban surface temperatures derived from satellite images. *International Journal of Remote Sensing*, *19*, 1639–1649.

Offerle, B., Grimmond, C. S. B., & Oke, T. R. (2003). Parameterization of net all-wave radiation for urban areas. *Journal of Applied Meteorology*, *42*, 1157–1173.

Oke, T.R. (2004). Initial guidance to obtain representative meteorological observations at urban sites, Instruments and Methods of Observation Programme, *IOM Report* No. 81, WMO/TD No. 1250, World Meteor. Organiz., Geneva. 51 pp. http://www.wmo.int/web/www/IMOP/publications/IOM-81/IOM-1E81-1EUrbanMetObs.pdf

Paw U, K. T. (1992). Development of models for thermal infrared radiation above and within plant canopies. *ISPRS Journal of Photogrammetry and Remote Sensing*, *47*, 189–203.

Schmid, H. P. (1997). Experimental design for flux measurements: Matching the scales of observations and fluxes. *Agricultural and Forest Meteorology*, *87*, 179–200.

Soux, C. A., Voogt, J. A., & Oke, T. R. (2004). A model to calculate what a remote sensor 'sees' of an urban surface. *Boundary - Layer Meteorology*, *111*, 109–132.

Verhoef, A., de Bruin, H. A. R., & van den Hurk, J. J. M. (1997). Some practical notes on the parameter kB21 for sparse vegetation. *Journal of Applied Meteorology*, *36*, 560–572.

Voogt, J. A., & Grimmond, C. S. B. (2000). Modeling surface sensible heat flux using surface radiative temperatures in a simple urban area. *Journal of Applied Meteorology*, *39*, 1679–1699.

Voogt, J. A., & Krayenhoff, E. S. (2005). Modeling urban thermal anisotropy. *5th International Symposium on Remote Sensing of Urban Areas (URS 2005), March 14–16 2005, Tempe, AZ, USA*.

Voogt, J. A., & Oke, T. R. (1997). Complete urban surface temperatures. *Journal of Applied Meteorology*, *36*, 1117–1132.

Voogt, J. A., & Oke, T. R. (1998). Effects of urban surface geometry on remotely-sensed surface temperature. *International Journal of Remote Sensing*, *19*, 895–920.

Voogt, J. A., & Oke, T. R. (1998). Radiometric temperatures of urban canyon walls obtained from vehicle traverses. *Theoretical and Applied Climatology*, *60*, 199–217.

Voogt, J. A., & Oke, T. R. (2003). Thermal remote sensing of urban climates. *Remote Sensing of Environment*, *86*, 370–384.

Glossary

Abbreviations and symbols used in the text

Abbreviation: Description

Sites

DT: Downtown study area
LI: Light Industrial study area

Acronyms

GIS: Geographic Information System
IFOV: Instantaneous field of view (°)
LST: Local standard time
RS: Roof structure
SUM: Surface-sensor-sun relations model

Symbol: Description (Unit)

A_c: Complete (3-D) area (m^2)
A_p: Plane (2-D) area (m^2)
A_r: Roof area (m^2)
A_{rd}: Road area (m^2)
A_{res}: Residual area (m^2)
A_{shd}: Shaded area (m^2)
F_{rd}: Fraction of road area in a sampled image
F_{shd}: Fraction of shaded area in a sampled image
T_r: Directional radiometric temperature (°C)
T_{rd}: Road (sunlit) temperature from image analysis (°C)
T_{res}: Residual temperature from image analysis (°C)
T_{shd}: Shaded (horizontal) surface temperature from image analysis (°C)